PROCEEDINGS OF SCIENCE

Charmless hadronic B decays

YoungMoon Goh*
Hanyang University
E-mail: ymgoh@hep.hanyang.ac.kr

ByungGu Cheon
Hanyang University
E-mail: bgcheon@hanyang.ac.kr

Yuuji Unno
Hanyang University
E-mail: yunno@post.kek.jp

This proceeding covers recent measurements of charmless hadronic B decays such as $B^+ \to \overline{K}^{*0}(892)K^{*+}(892)$, $B^0 \to \omega\omega/\omega\phi$, $B^0 \to \pi^0\pi^0$, $B^0 \to \eta\pi^0$, $B^0 \to \rho^0\rho^0$ and $B^+ \to K^0_S\pi^+\pi^-$ reported from Belle, BaBar and LHCb experiments. In the $B^+ \to \overline{K}^{*0}(892)K^{*+}(892)$ decay channel, Belle found a 2.7σ excess of signal, which correspond to the branching fraction $\mathscr{B} = (0.77^{+0.35}_{-0.30} \pm 0.12) \times 10^{-6}$ and the longitudinal polarization fraction $f_L = 1.06 \pm 0.30 \pm 0.14$. In BaBar, the $B^0 \to \omega\omega$ is measured with the $\mathscr{B} = (1.2 \pm 0.3^{+0.3}_{-0.2}) \times 10^{-6}$ and the $\mathscr{B}$ upper limit of $B^0 \to \omega\phi$ is set to 0.7×10^{-6} at the 90% confidence-level. Belle reports an updated measurement of $\mathscr{B} = (0.90 \pm 0.12 \pm 0.10) \times 10^{-6}$ in the $B^0 \to \pi^0\pi^0$ and the first measurement of $\mathscr{B} = (4.1^{+1.7+0.5}_{-1.5-0.7}) \times 10^{-7}$ in $B^0 \to \eta\pi^0$. The $\mathscr{B} = (0.94 \pm 0.17 \pm 0.09 \pm 0.06) \times 10^{-6}$ and the $f_L = 0.745^{+0.048}_{-0.058} \pm 0.034$ are precisely measured by LHCb, where the $\mathscr{B}$ last uncertainty is due to the $B^0 \to \phi K^{*0}$ reference mode. Finally the difference between CP asymmetries of $K^*\pi$ intermediate states is reported as $A_{CP}(K^{*+}\pi^0) - A_{CP}(K^{*+}\pi^-) = -0.16 \pm 0.13$ by BaBar.

Flavor Physics & CP Violation 2015,
May 25-29, 2015
Nagoya, Japan

*Speaker.

PoS(FPCP2015)007

1. Introduction

The $b \to c$ decays take an order of 99% of all B decays, while the others are considered as charmless and rare decays. Those charmless B decays probe dynamics of weak and strong interactions [1]. In these decays, the interference between penguin and tree diagrams can lead to the direct CP violation, and the relative weak phase of tree and penguin can also give the unitarity triangle angles in the Cabibbo-Kobayashi-Maskawa (CKM) matrix. These allow searches for new physics from the new particles by looking for the enhanced branching fraction ($\mathscr{B}$), CP asymmetry (A_{CP}), and so on. Analyses of Belle and BaBar used the data samples taken at the $\Upsilon(4S)$ resonance, corresponding to integrated luminosities of 711 fb^{-1} and 429 fb^{-1}, respectively. The analysed data in LHCb corresponds to an integrated luminosity of 3.0 fb^{-1} from pp collisions.

2. Analysis of $B^+ \to \overline{K}^{*0}(892)K^{*+}(892)$ in Belle and $B^0 \to \omega\omega/\omega\phi$ in BaBar

The polarization puzzle for $B \to VV$ decay channels has yet to be solved due to a baffling pattern in the longitudinal polarization fraction (f_L); here, V denotes a vector meson. Many of those decay channels with the $b \to d$ transition have still large uncertainties for the f_L. Therefore, precise measurements of $B^+ \to \overline{K}^{*0}(892)K^{*+}(892)$ and $B^0 \to \omega\omega/\omega\phi$ mediated by $b \to d$ transitions based on high statistics are needed to shed more light on the polarization puzzle.

The $B^+ \to \overline{K}^{*0}K^{*+}$ candidate is reconstructed from the subsequent decay channels of $\overline{K}^{*0} \to K^-\pi^+$ and $K^{*+} \to K^+\pi^0$ ($K^0_S\pi^+$), where K^* refers to the $K^*(892)$ meson, and the $B^0 \to \omega\omega/\omega\phi$ candidate is reconstructed from $\omega \to \pi^+\pi^-\pi^0$ and $\phi \to K^+K^-$, with $K^0_S \to \pi^+\pi^-$ and $\pi^0 \to \gamma\gamma$. Charged tracks are reconstructed by using the standard particle identification criteria with additional selections such as the transverse momentum. The π^0 candidates are reconstructed with an invariant mass requirement corresponding to about 3σ around the nominal π^0 mass [2]. The K^0_S candidates have to suffice the standard impact parameter criteria and have an invariant mass ranged from 0.478 GeV/c^2 to 0.516 GeV/c^2. Selection requirements on the invariant mass of B-daughter intermediate states for K^*, ω, and ϕ are 0.78 GeV/c^2 $< m_{K\pi} <$ 1.0 GeV/c^2, 0.74 GeV/c^2 $< m_{\pi\pi\pi} <$ 0.82 GeV/c^2, and 1.009 GeV/c^2 $< m_{KK} <$ 1.029 GeV/c^2.

Two kinematic observables are defined in the form of the energy difference ($\Delta E \equiv E_B - E_{\rm beam}$) and the beam-energy constrained mass ($M_{bc}(m_{ES}) \equiv \frac{1}{c^2}\sqrt{E^2_{\rm beam} - |\vec{p}_B|^2c^2}$), where $E_{\rm beam}$ and E_B ($\vec{p}_B$) are the beam energy and the energy (momentum) of the B meson candidate, respectively, in the e^+e^- center-of-mass (CM) frame. For the $K^{*+} \to K^+\pi^0$ channel of $B^+ \to \overline{K}^{*0}K^{*+}$, where the ΔE resolution is poor due to shower leakage in the electromagnetic calorimeter (ECL) [3], the modified beam constrained mass M^*_{bc} is used, which takes into account only the π^0 direction but not also its energy. B candidates satisfy that $|\Delta E| < 0.15$ GeV and $M^{(*)}_{\rm bc} > 5.25$ GeV/c^2 for the $B^+ \to \overline{K}^{*0}K^{*+}$, $|\Delta E| < 0.2$ GeV and $m_{ES} > 5.24$ GeV/c^2 for the $B^0 \to \omega\omega/\omega\phi$.

The dominant source of background for both decay channels is the $e^+e^- \to q\bar{q}$ ($q \in \{u,d,s,c\}$) continuum process. A neural network (NN) implemented with the NeuroBayes (NB) package [4] in the $B^+ \to \overline{K}^{*0}K^{*+}$ and a Fisher discriminant ($\mathscr{F}$) [5] in the $B^0 \to \omega\omega/\omega\phi$ are employed by combining event topology variables to suppress this background. The NN output (C_{NB}) is transformed into an analytic shape (C'_{NB}) to enable its modeling with disregarding candidates having $C_{NB} < -0.5$, where C_{NB} is ranged from -1 to 1. The $B\bar{B}$ backgrounds are also taken into

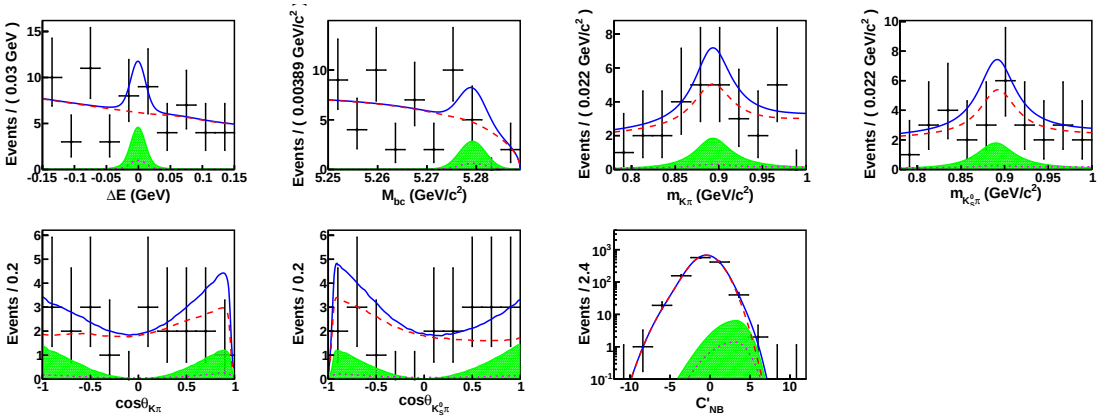

Figure 1: (color online). Projections for $B^+ \to \overline{K}^{*0}(\to K^-\pi^+)K^{*+}(\to K^0_S\pi^+)$ of the multidimensional fit onto ΔE, M_{bc}, $\overline{K}^{*0}$ mass, K^{*+} mass, cosine of $\overline{K}^{*0}$ helicity angle, cosine of K^{*+} helicity angle, and C'_{NB} for events selected in a signal enhanced region with the plotted variable excluded. Points with error bars are the data, the solid curves represent the full fit function, the hatched regions are the signal, the dashed curves show the combined continuum and $B\bar{B}$ backgrounds, and the dotted curves are the higher K^* and nonresonant backgrounds.

account to two categories of backgrounds having combinatorial and peaking structures on ΔE and $M_{bc}(m_{ES})$. $(\overline{K}\pi)^{*0}_0 K^{*+}$, $\overline{K}^{*0}(K\pi)^{*+}_0$ and four-body decays contribute to peaking structures for the $B^+ \to \overline{K}^{*0}K^{*+}$, while $\omega\omega\pi^0$, $\omega\phi\pi^0$, $\omega\rho\pi$, and ωa_1 decays contribute to them for the $B^0 \to \omega\omega/\omega\phi$.

The extended unbinned maximum-likelihood fits are performed to extract both $\mathscr{B}$ and f_L for the $B^+ \to \overline{K}^{*0}K^{*+}$, and to extract the $\mathscr{B}$ for the $B^0 \to \omega\omega/\omega\phi$ by fixing a parameter $f_L = 0.88$. These fits include seven input observables ΔE, beam-energy constrained mass, two vector-meson invariant masses, two vector-meson helicity angles, and continuum suppression variable. In addition, for the $B^0 \to \omega\omega/\omega\phi$, a helicity angle ($\Phi$) for each ω is provided by the polar angle of the π^0 in the $\pi^+\pi^-$ rest frame with respect to the ω flight direction. The distribution of this extra fit variable, $\cos\Phi_\omega$, is proportional to $1-\cos^2\Phi_\omega$ for signal, while nearly flat for background.

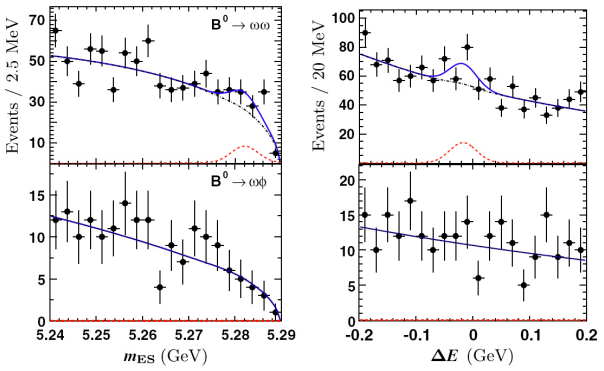

Figure 2: (color online). Projections for $B^0 \to \omega\omega$ (upper plots) and $B^0 \to \omega\phi$ (lower plots) onto m_{ES} (left) and ΔE (right) for events selected in a signal enhanced region with the plotted variable excluded. Points with error bars are the data, the solid curves represent the full fit function, the dashed curves show the signal, and the dot-dashed curves are the background.

In the $B^+ \to \overline{K}^{*0}K^{*+}$, the fit is performed simultaneously to both channels of $K^{*+} \to K^0_S\pi^+$ and $K^{*+} \to K^+\pi^0$.

Figure 1 shows the signal-enhanced projections of seven-dimensional fit variables for the $B^+ \to \overline{K}^{*0}K^{*+}$ decay channel, where the signal-enhanced regions are ranged by $|\Delta E| < 0.05$ GeV, $M^{(*)}_{\rm bc} > 5.27$ GeV$/c^2$, 0.83 GeV$/c^2 < m_{K\pi} < 0.95$ GeV$/c^2$ and $C'_{NB} > 3$. Figure 2 shows the signal-enhanced projections of m_{ES} (left) and ΔE for the $B^0 \to \omega\omega/\omega\phi$ decay channel, where the signal-enhanced regions are ranged by $|\Delta E| < 0.03$ GeV, $m_{ES} > 5.274$ GeV$/c^2$, $|m_{\pi\pi\pi} - m^{\rm nominal}_{\omega}| < 0.015$ GeV$/c^2$, $|m_{KK} - m^{\rm nominal}_{\phi}| < 0.015$ GeV$/c^2$, $\mathscr{F} < 0.1$, $|\cos\Phi_{\pi\pi\pi}| < 0.95$, and $|\cos\theta_{\rm T}| < 0.8$.

The dominant systematic uncertainties for $\mathscr{B}$ and f_L measurements in the $B^+ \to \overline{K}^{*0}K^{*+}$ are arisen from the fit bias, probability density function (PDF) modelings, estimations of nonresonant and higher K^* background, and interference with $(K\pi)^*_0$. In total, $^{+16.2}_{-15.4}$ % and $^{+13.7}_{-13.9}$ % uncertainties are determined for the $\mathscr{B}$ and the f_L, respectively. The total $\mathscr{B}$ systematic uncertainties for $B^0 \to \omega\omega$ and $B^0 \to \omega\phi$ are $^{+26.3}_{-9.7}$ % and $^{+31.5}_{-69.5}$ %, respectively, due to the fit bias, f_L variations, and vertex finding efficiencies.

Including systematic uncertainties, a $B^+ \to \overline{K}^{*0}K^{*+}$ signal of $15.8^{+7.2}_{-6.1}$ ($K^0_S\pi^+$) and $16.7^{+7.6}_{-6.5}$ ($K^+\pi^0$) with 2.7σ significance is observed, with corresponding to $\mathscr{B} = (0.77^{+0.35}_{-0.30} \pm 0.12) \times 10^{-6}$ and $f_L = 1.06 \pm 0.30 \pm 0.14$ [6]. This $\mathscr{B}$ upper limit is 1.31×10^{-6} at 90% CL. Including systematic uncertainties, a $B^0 \to \omega\omega$ signal of $69.0^{+16.4}_{-15.2}$ with 4.4σ significance is observed, with corresponding to $\mathscr{B} = (1.2 \pm 0.3^{+0.3}_{-0.2}) \times 10^{-6}$, and the $\mathscr{B}$ upper limit of $B^0 \to \omega\phi$ is set to 0.7×10^{-6} at 90% CL [7].

3. Analysis of $B^0 \to \pi^0\pi^0$ and $B^0 \to \eta\pi^0$ in Belle

The time dependent CP asymmetries in the $B^0 \to \pi^+\pi^-$ decay is used to measure an angle ϕ_2 parameter in the CKM matrix. However, this angle cannot be easily extracted due to the penguin diagram contribution. We overcome this by using the isospin analysis of $\pi\pi$ system [8] for the $\mathscr{B}$ and A_{CP}. The $B^0 \to \pi^0\pi^0$ decay is needed for this isospin relation and the $B^0 \to \eta\pi^0$ decay can be used to constrain the isospin-breaking effects on $\sin\phi_2$ [9, 10].

The $B^0 \to \pi^0\pi^0$ candidates are reconstructed from a π^0 pair and the $B^0 \to \eta\pi^0$ candidates are reconstructed from η and π^0, where channels of $\pi^0 \to \gamma\gamma$ and $\eta \to \gamma\gamma(\eta_{\gamma\gamma})/\pi^+\pi^-\pi^0(\eta_{3\pi})$ are taken. We require that the reconstructed photon energy is greater than 50 MeV in the barrel and 100 MeV in the endcap region of the ECL. The invariant mass of two photon combination has to suffice 115 MeV$/c^2 < m_{\gamma\gamma} <$ 152 MeV$/c^2$ for the $B^0 \to \pi^0\pi^0$ and 115 MeV$/c^2 < m_{\gamma\gamma} <$ 155 MeV$/c^2$ for the $B^0 \to \eta\pi^0$ with requiring $\chi^2 < 50$ from the π^0 mass-constrained fit. The requirement of $|E_1 - E_2|/|E_1 + E_2| < 0.9$ for photon energies of $\eta_{\gamma\gamma}$ is applied to reduce combinatorial background due to the low-energy photons, where E_1 and E_2 are two photon energies. For the charged tracks from $\eta_{3\pi}$, the standard particle identification criteria and the impact parameter criteria are required. The invariant mass ranges of $\eta_{\gamma\gamma}$ and $\eta_{3\pi}$ candidates are 500 MeV$/c^2 < m_{\eta_{\gamma\gamma}} <$ 575 MeV$/c^2$ and 538 MeV$/c^2 < m_{\eta_{3\pi}} <$ 557 MeV$/c^2$. All candidates satisfy that $M_{\rm bc} > 5.26$ GeV$/c^2$ and -0.3 GeV$< \Delta E <$ 0.2 GeV for the $B^0 \to \pi^0\pi^0$, and $M_{\rm bc} > 5.24$ GeV$/c^2$ and -0.30 GeV$< \Delta E <$ 0.25 GeV for the $B^0 \to \eta\pi^0$.

In order to suppress continuum events, the NB and the $\mathscr{F}$ techniques are used with disregarding candidates in regions $C_{NB} < -0.1$ and $\mathscr{F} < -0.3$ for $B^0 \to \pi^0\pi^0$ and $B^0 \to \eta\pi^0$, respectively,

where C_{NB} and $\mathscr{F}$ are ranged from -1 to 1. The $B\bar{B}$ peaking backgrounds due to out-of-timing ECL events are removed by a ECL timing cut.

The extended unbinned maximum-likelihood fits are performed to extract the $\mathscr{B}$ for three variables: ΔE, $M_{\rm bc}$, and continuum suppression variable. Figure 3 shows the signal-enhanced projections of three fit variables for the $B^0 \to \pi^0\pi^0$ decay channel, where the signal-enhanced region are ranged by -0.15 GeV$< \Delta E < 0.05$ GeV and 5.275 GeV$/c^2 < M_{\rm bc} < 5.285$ GeV$/c^2$. Figure 4 shows the signal-enhanced projections of three fit variables for the $B^0 \to \eta\pi^0$ decay channel, where the signal-enhanced region are ranged by -0.21 GeV$< \Delta E < 0.15$ GeV, 5.27 GeV$/c^2 < M_{\rm bc}$ and $C'_{NB} > 1.5$.

For the $B^0 \to \pi^0\pi^0$ decay, the signal yield of 225 ± 30 events (statistical error only) is found, and the 11% systematic uncertainty for $\mathscr{B}$ is assigned due to the efficiency assumption of input $\mathscr{B}$, the PDF parametrization and the timing cut efficiency. The $\mathscr{B}$ is determined to be $\mathscr{B} = (0.90 \pm 0.12 \pm 0.10) \times 10^{-6}$ with a significance of 6.7σ. This is the first measurement of $\mathscr{B}$ using timing information from the ECL.

For the $B^0 \to \eta\pi^0$ decay, the signal yields of $30.6^{+12.2}_{-10.8}$ and $0.5^{+6.6}_{-5.4}$ events (statistical error only) are found for $\eta_{\gamma\gamma}\pi^0$ and $\eta_{3\pi}\pi^0$, respectively, and $^{+12.2}_{-15.9}$% systematic uncertainties for $\mathscr{B}$ are assigned due to the PDF parametrization, the $\pi^0/\eta \to \gamma\gamma$ reconstruction, and nonresonant contributions. The $\mathscr{B}$ is determined to be $\mathscr{B} = (4.1^{+1.7+0.5}_{-1.5-0.7}) \times 10^{-7}$ with a significance of 3.0σ [11]. From Ref [9] with this $\mathscr{B}$ value, the isospin-breaking correction to the weak phase ϕ_2 measurement

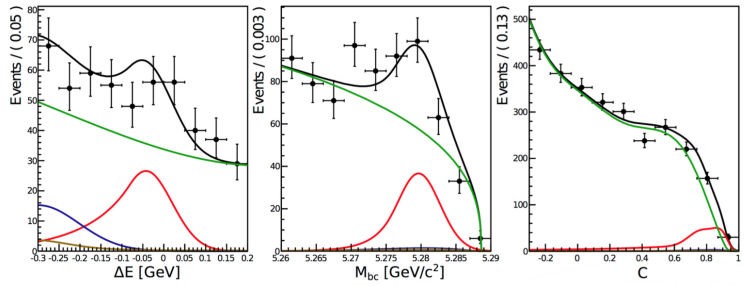

Figure 3: (color online). Projections for $B^0 \to \pi^0\pi^0$ on ΔE, $M_{\rm bc}$, and C for events selected in a signal enhanced region with the plotted variable excluded. Points with error bars are the data and the solid curves represent the full fit function. Contributions from signal, continuum, $b \to u,d,s$ charmless rare $B\bar{B}$, and $B \to \rho\pi$ are shown with red, brown, and blue lines, respectively.

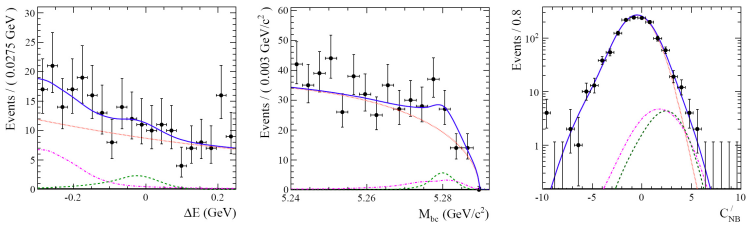

Figure 4: (color online). Projections for $B^0 \to \eta\pi^0$ ($\eta \to \gamma\gamma$) on ΔE, $M_{\rm bc}$, and C'_{NB} for events selected in a signal enhanced region with the plotted variable excluded. Points with error bars are the data and the solid curves represent the full fit function. The dahsed, dotted, and dot-dashed curves represent the signal, continuum, and charmless rare B backgrounds, respectively.

in the $B \to \pi\pi$ due to $\pi^0 - \eta - \eta'$ mixing is estimated less than 0.97° at 90% CL.

4. Analysis of $B^0 \to \rho^0\rho^0$ in LHCb

The Belle and BaBar experiments reported the evidence for the $B^0 \to \rho^0\rho^0$ decay [12, 13] with the f_L measurements. However, its results of both experiments differ at the level of 2.0 standard deviations. The large LHCb dataset may shed light on this discrepancy.

At least one charged particle should have the transverse momentum ($p_{\rm T}$) greater than 1.7 GeV/c and the inconsistency with originating from any primary interaction. For the b hadron decay selection, a multivariate algorithm [14] is used for the identifiaction of secondary vertices for those decay. Further selection criteria has the transverse momentum of $(\pi^+\pi^-)$ candidates greater than 0.6 GeV/c, with at least one charged decay product with $p_{\rm T} > 1$ GeV/c, the transverse momentum of B^0 candidates reconstructed from two $(\pi^+\pi^-)$ pairs greater than $p_{\rm T} > 2.5$ GeV/c, the range from 0.3 GeV/c^2 to 1.1 GeV/c^2 for the invariant mass of $(\pi^+\pi^-)$ candidates, and the range from 5.05 GeV/c^2 to 5.5 GeV/c^2 for the invariant mass of B^0 candidates. The identification of the final-state particles (PID) is performed with dedicated neural-networks-based discriminating variables [15] and a boosted decision tree algorithm (BDT) is used to suppress the combinatorial background [16, 17].

An unbinned extended likelihood fit for the four-body mass spectrum $M(\pi^+\pi^-)(\pi^+\pi^-)$ is performed simultaneously together with the normalization channel $M(K^+K^-)(K^+\pi^-)$ and the PID misidentification control channel $M(K^+\pi^-)(\pi^+\pi^-)$ mass spectra. The $M(\pi^+\pi^-)(\pi^+\pi^-)$ spectrum is first analyzed with the *sPlot* technique [18] to subtract statistically the background under the $B^0 \to (\pi^+\pi^-)(\pi^+\pi^-)$ signal . We consider decay channels from B^0 to $\rho^0\rho^0$ and $\omega\rho^0$ for $B \to VV$, $\rho^0\rho^0(\pi^+\pi^-)_0$ and $\rho^0 f_0(980)$ for $B \to VS$, longitudinal $\rho^0 f_2(1270)$ for $B^0 \to VT$, $B^0 \to SS$, and $B^0 \to a_1^\pm\pi^\pm$ along with its interference to other amplitudes. Distributions and fit projections of those decays are shown in Figure 5 on subtracted invariant mass and cosine of helicity angle of a pion pair, and azimuthal angle between helicity planes of two pion pairs. Systematic uncertainties comes from mostly the limited size of simulated events samples, discrepancies between experimental and simulated data, efficiencies of PID requirements, and tracking efficiencies for π and K.

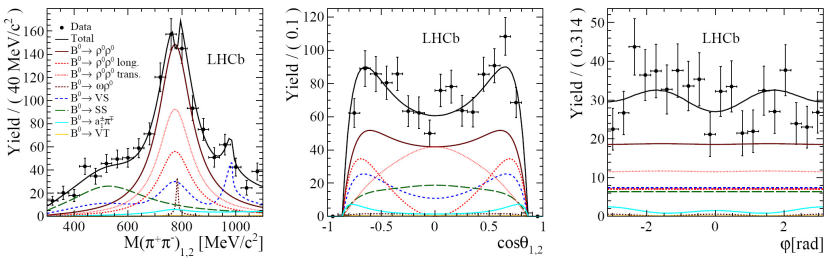

Figure 5: (color online). Projections for $B^0 \to \rho^0\rho^0$ on background-subtracted $M(\pi^+\pi^-)$, cosθ and φ distributions. Points with error bars are the data and the solid curves represent the full fit function. The specific decays $B^0 \to \rho^0\rho^0$ (solid brown), longitudinal $B^0 \to \rho^0\rho^0$ (dashed red), transverse $B^0 \to \rho^0\rho^0$ (dotted red), $B^0 \to \omega\rho^0$ (dashed brown), $B^0 \to VS$ (dashed blue), $B^0 \to SS$ (long dashed green), $B^0 \to VT$ (orange) and $B^0 \to a_1^\pm\pi^\pm$ (light blue) are displayed.

After performing the unbinned extended likelihood fit to the angular and two-body invariant mass distributions, a $B^0 \to \rho^0\rho^0$ signal of $634 \pm 28 \pm 8$ with 7.1σ significance is observed, with corresponding to $\mathscr{B} = (0.94 \pm 0.17 \pm 0.09 \pm 0.06) \times 10^{-6}$, where the last uncertainty is due to the normalization channel, and $f_L = 0.745^{+0.048}_{-0.058} \pm 0.034$ [19]. This measurement is the first observation.

5. Dalitz plot analysis of $B^+ \to K^0_S\pi^+\pi^0$ in BaBar

Tree amplitudes in $B \to K^*\pi$ decays as intermediated states of $K^{*0}\pi^+$ and $K^{*+}\pi^0$ are populated from the Dalitz plane. Those decays are sensitive to the ϕ_3 angle. This angle can be obtained from a relative phase $\Phi_{3/2} = -\frac{1}{2}\mathrm{Arg}\left(\bar{\mathrm{A}}_{3/2}/\mathrm{A}_{3/2}\right)$ in absence of the electroweak penguin contributions [20], where $A_{3/2}$ is constructed from a linear combination of weak decay amplitudes for the $B \to K^*\pi$ to form a pure isospin $I = 3/2$, and $\bar{A}_{3/2}$ is the CP conjugate of the $A_{3/2}$. In this isospin analysis, QCD penguin contributions are eliminated [21].

The $B^+ \to K^0_S\pi^+\pi^0$ candidate is reconstructed from candidates of a π^0, a charged pion, and a K^0_S with a pair of charged pions in selection requirements, where the π^0 laboratory energy is above 0.05 GeV, the π^0 lateral moments are between 0.01 and 0.6, the π^0 invariant mass range is from 0.11 GeV/c^2 to 0.16 GeV/c^2, the K^0_S invariant mass is ranged ± 15 MeV/c^2 around the K^0_S nominal mass, the K^0_S proper decay time is greater than $0.5 \times 10^{-11}s$, the K^0_S vertex probability is greater than 10^{-6}, the cosine of the angle between the momentum and the flight directions of K^0_S is greater than 0.995, and standard particle identification criteria are used for charged pions. $|\Delta E| < 0.3$ GeV and $m_{ES} > 5.23$ GeV/c^2 are also required for the selection of B candidates.

In order to suppress continuum events, the BDT algorithm is used with disregarding candidates having BDT output less than 0.06. The charmed $B\bar{B}$ background such as $B^+ \to \bar{D}^0\pi^+$ is vetoed with $1.804\ \mathrm{GeV}/c^2 < m_{K^0_S\pi^0} < 1.924\ \mathrm{GeV}/c^2$. The remaining $B\bar{B}$ backgrounds are classified based on the shape of five fit variables Δ, m_{ES}, and Dalitz plot distriubtions of $m^2_{K^0_S\pi^+}$ and $m^2_{\pi^+\pi^0}$.

An unbinned extended likelihood fit with the Laura++ software [22] is performed for five fit variables into simultaneously $B^\pm$ with fit components $K^0\pi^+\pi^0$, $K^{*0}\pi^+$, $K^{*+}\pi^0$, $K^{*0}(1430)\pi^+$, $K^{*+}(1430)\pi^0$, ρ^+K^0, continuum and $B\bar{B}$ background. In systematics, dominant uncertainties are originated from the BDT output PDF modeling, self crossfeed signal PDF modeling, background model in the Dalitz plot, the Blatt-Weisskopf radius parameter [23], and parameters of $K^*(892)$ and $K^*_0(1430)$.

In this study, the first $\mathscr{B}$ measurements of $K^0\pi^+\pi^0$ and $K^{*+}(1430)\pi^0$ are obtained as $(45.9 \pm 2.6 \pm 3.0^{+8.6}_{-0.0}) \times 10^{-6}$ and $(17.2 \pm 2.4 \pm 1.5^{+0.0}_{-1.8}) \times 10^{-6}$, respectively [24], where the last uncertainty is due to the signal model. The first evidence of A_{CP} in the $B^+ \to K^{*+}\pi^0$ is also found as $-0.52 \pm 0.14 \pm 0.04^{+0.04}_{-0.02}$ corresponding to the significance 3.4σ. Together with pervious measurements [25] for $K^*\pi$, averaged difference of A_{CP}s are estimated with $\Delta A_{CP}(K^*\pi) \equiv A_{CP}(K^{*+}\pi^0) - A_{CP}(K^{*+}\pi^-) = -0.16 \pm 0.13$. Although this analysis makes this uncertainty much improved, this is still too large to be conclusive. The $K^*\pi$ relative phase uncertainty is also too large to measure the ϕ_3 in this statistics.

Acknowledgments

We acknowledge support from the National Research Foundation of Korea Grant No. 2015R1A2A2A01003280.

References

[1] R. Fleischer and M. Gronau, Phys. Lett. B **660**, 212 (2006); Z. Xiao, C. S. Li and K.-T. Chao, Phys. Rev. D **63**, 074005 (2001); W. Zou and Z. Xiao, Phys. Rev. D **72**, 094026 (2005).

[2] K. A. Olive *et al.* (Particle Data Group), Chin. Phys. C **38**, 090001 (2014).

[3] A. Abashian *et al.* (Belle Collaboration), Nucl. Instrum. Methods Phys. Res., Sect. A **479**, 117 (2002); also, see the detector section in J. Brodzicka *et al.*, Prog. Theor. Exp. Phys., 04D001 (2012).

[4] M. Feindt and U. Kerzel, Nucl. Instrum. Methods Phys. Res., Sect. A **559**, 190 (2006).

[5] R. A. Fisher, Ann. Eugenics **7**, 179 (1936).

[6] Y. M. Goh *et al.* (Belle Collaboration), Phys. Rev. D **91**, 071101 (2015).

[7] J. P. Lees *et al.* (BABAR Collaboration), Phys. Rev. D **89**, 051101 (2014).

[8] M. Gronau, D. London, Phys.Rev.Lett. **65**, 33813384 (1990).

[9] M. Gronau and J. Zupan, Phys. Rev. D **71**, 074017 (2005).

[10] S. Gardner, Phys. Rev. D **72**, 034015 (2005).

[11] B. Pal *et al.* (Belle Collaboration), arXiv:1504.00957 (2015).

[12] B. Aubert *et al.* (BABAR Collaboration), Phys. Rev. D **78**, 071104 (2008).

[13] P. Vanhoefer *et al.* (Belle Collaboration), Phys. Rev. D **89**, 072008 (2014).

[14] V. V. Gligorov and M. Williams, JINST **8**, P02013 (2013).

[15] M. Adinolfi *et al.* (LHCb RICH Collaboration), Eur. Phys. J. C**73**, 2431 (2013).

[16] L. Breiman, J. H. Friedman, R. A. Olshen, and C. J. Stone, *Classification and regression trees*, Wadsworth international group, Belmont, California, USA (1984).

[17] R. E. Schapire and Y. Freund, Jour. Comp. and Syst. Sc. **55**, 119 (1997).

[18] M. Pivk and F. R. Le Diberder, Nucl. Instrum. Meth. A**555**, 356 (2005).

[19] R. Aaij *et al.* (LHCb collaboration), arXiv:1503.07770 (2015).

[20] M. Gronau, D. Pirjol, A. Soni, and J. Zupan, Phys. Rev. D **75**, 014002 (2007).

[21] M. Ciuchini, M. Pierini, and L. Silvestrini, Phys. Rev. D **74**, 051301 (2006).

[22] T. Latham, J. Back, and P. Harrison, Laura++, http://laura.hepforge.org.

[23] J. Blatt and V. Weisskopf, *Theoretical Nuclear Physics*, J. Wiley and sons, New York (1952).

[24] J. P. Lees *et al.* (BABAR Collaboration), arXiv:1501.00705 (2015).

[25] J. Dalseno *et al.* (Belle Collaboration), Phys. Rev. D **79**, 072004 (2009); J.P. Lees *et al.* (BABAR Collaboration), Phys.Rev. D **83**, 112010 (2011); Phys.Rev. D **84**, 092007 (2011).